

Effects of Strain Accumulation on the Superplastic Deformation Behavior of 7075 AL Alloy

Y. Kwon and Y. Chang

(Submitted 2 December 1999)

The superplastic deformation behavior of a fine-grained 7075 Al alloy has been investigated within the framework of an internal variable theory for inelastic deformation. The theory takes the dislocation glide process within and across the grain boundaries (grain matrix deformation (GMD)) as the major accommodation mechanism for the grain boundary sliding (GBS). The flow curves were obtained by performing a series of load relaxation tests at the various prestrain values to examine the effects of accumulated strain on the superplastic deformation behavior. The most significant result obtained in this study is that the grain boundary characteristics change gradually with the strain accumulation from an initially Newtonian viscous flow signified with the power index value of $M_g = 1$ to a non-Newtonian flow with the value of $M_g = 0.5$ commonly observed in the various microduplex alloys such as Ti-6Al-4V. The variation of GBS characteristics with the prestrain is then examined by observing the microstructural evolution with the strain through the use of transmission electron microscopy (TEM).

Keywords aluminum alloy 7675, grain boundary sliding, strain rate, superplasticity

1. Introduction

Superplasticity is typically characterized as the ability for crystalline materials to exhibit an extensive tensile elongation prior to failure.[1] Most of the studies have attempted to analyze the superplastic flow behavior based on a single power law relation between the flow stress σ and the strain rate $\dot{\varepsilon}$ with the strain rate sensitivity m. Further, the value of m, which is the slope of log σ versus log $\dot{\varepsilon}$, has been considered as a unique parameter for superplasticity.

It is well known that the superplastic deformation is often accompanied by microstructural evolutions such as grain growth and cavitation.[2,3] Also, there has been a report that the strain rate sensitivity changes with strain.[4] Therefore, it is thought to be no longer valid to attempt to analyze the superplastic flow as a steady-state deformation behavior, which has been assumed through the great deal of research done on superplasticity. Because a large amount of strain is encountered during the superplastic forming processes, however, the evolution of superplastic deformation behavior with the strain has to be clearly characterized.

A new internal variable theory has recently been proposed to provide a more comprehensive understanding of the superplastic deformation behavior.[5] The basic theme of this theory is that superplastic deformation consists of grain boundary sliding (GBS) and an accommodating grain matrix deformation (GMD) by dislocation slip. The following relations were developed from the model:[5]

$$\dot{\varepsilon} = \dot{\mathring{a}} + \dot{a} + \dot{g} \qquad \text{(Eq 1)}$$

$$\sigma = \sigma^I + \sigma^F \qquad \text{(Eq 2)}$$

$$(\sigma^*/\sigma^I) = \exp(\dot{a}^*/\dot{a})^p \qquad \text{(Eq 3)}$$

$$(\dot{g}/\dot{g}_0) = (\sigma/\Sigma_g - 1)^{1/M_g} \qquad \text{(Eq 4)}$$

Equation 3 and 4 are the constitutive relations for plastic deformation by dislocation process and GBS, respectively. The parameters p and M_g are material constants, and σ^* and $\dot{\alpha}^*$ are the internal strength variable and its conjugate reference strain rate, while the parameters Σ_g and $\dot{g}_0$ denote the frictional resistant stress and its conjugate reference strain rate for GBS, respectively.

The present study has been carried out to examine the effect of strain on the flow behavior of a fine-grained 7075 Al alloy. Load relaxation tests were then carried out for a 7075 Al alloy with the increment of strain at 515 °C to obtain the evolution of deformation characteristics with strain. These flow curves are then separated into the GMD curve and the GBS curve, as prescribed by the theory and analyzed thoroughly. The microstructural observations were also carried out to investigate the evolution of microstructural characteristics with strain. Finally, the results obtained from the analysis of each flow curve are discussed in relation to the microstructural characteristics. It is believed possible to extract more valuable information about the effect of the strain accumulation on the superplastic deformation behavior from this approach, which has not been possible to obtain from the conventional approach.

2. Experimental Procedures

A commercial grade 7075 Al alloy was obtained in the form of 30 mm thick plate with the chemical compositions of 5.76Zn, 1.96Mg, 1.61Cu, 0.22Cr, 0.04Mn, and 0.19Fe by weight percent. A thermomechanical treatment process has been carried out to produce the fine-grained microstructure, and the final grain sizes of a 7075 Al alloy used in the present study are 7.1

Y. Kwon and **Y. Chang,** Center for Advanced Aerospace Materials (CAAM), Pohang University of Science and Technology (POSTECH), Pohang 790-784, Korea. Contact e-mail: kyn@postech.ac.kr.

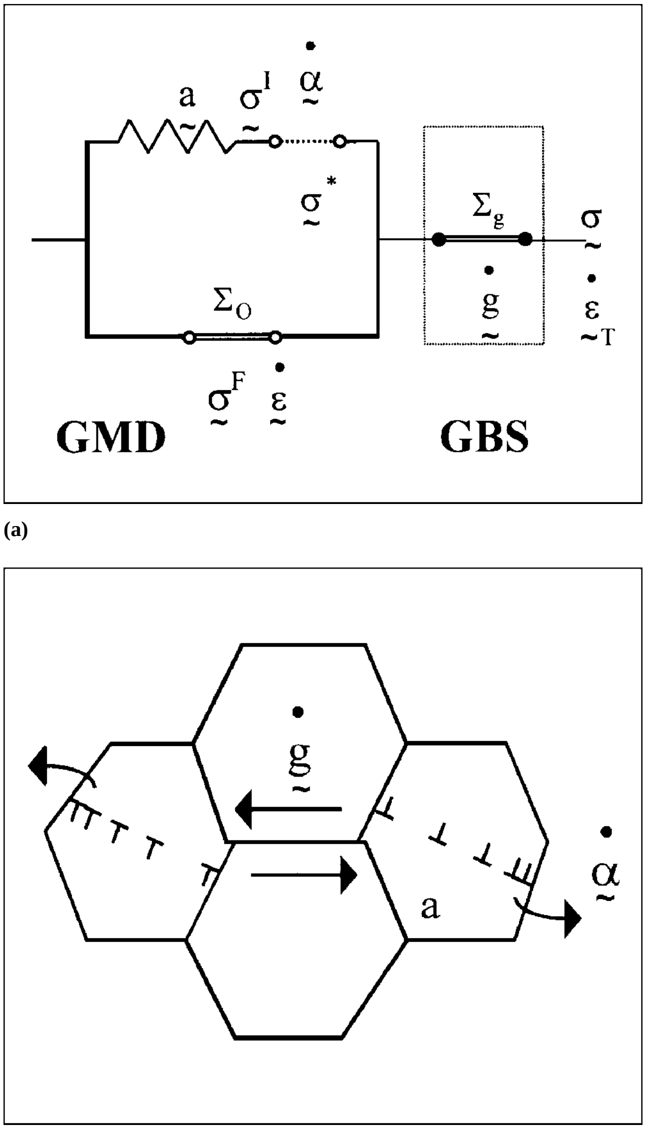

(a)

(b)

Fig. 1 An internal variable model for structural superplasticity: (**a**) rheological model and (**b**) physical model

μm for load relaxation tests and 5.6 μm for the microstructural observations, respectively.

Load relaxation tests were conducted to obtain the flow curves of a 7075 A1 alloy with the increment of strain at 515 °C. The strain rate of tensile deformation between each load relaxation test was chosen as $\dot{\varepsilon} = 1 \times 10^{-4}$/s to provide the stable deformation of tensile specimens without necking. The constant strain rate tensile tests were also carried out to obtain the specimens that were used for the microstructure at 510 °C.

Metallographic examinations were then conducted using scanning electron microscopy and transmission electron microscopy (TEM) to investigate the evolutions of microstructural characteristics with the increment of strain. Thin foils for TEM were prepared by the electrolytic polishing solution containing 34% nitric acid in methanol at 243 K and were examined in a Philips CM300 transmission electron microscope (Philips Electronic Instruments Corp., Mahwah, NJ) operating at 300 kV.

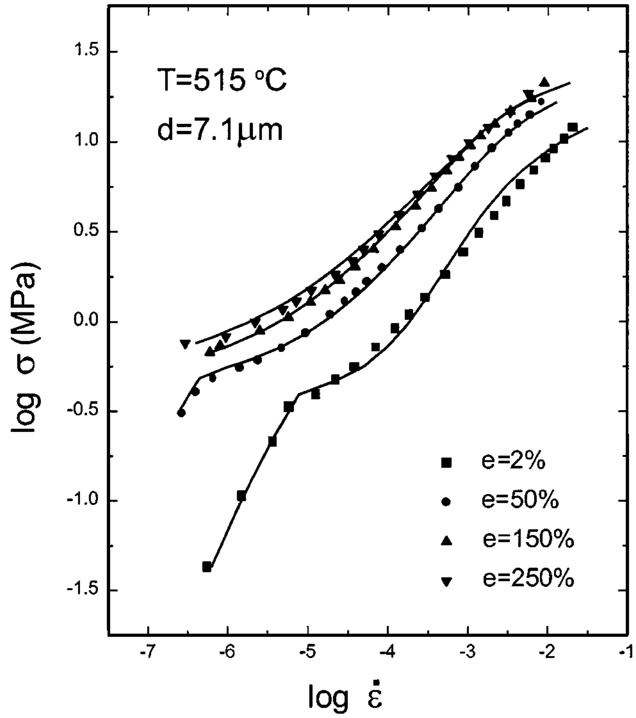

Fig. 2 The flow curves of a 7075 Al alloy with the increment of strain are obtained from load relaxation tests at $T = 515$ °C. The solid lines represent the predicted curves

3. Experimental Results and Analysis

3.1 Analysis of Flow Curves

The strain dependence of flow behavior is shown in Fig. 2, where the flow stress σ is plotted against the inelastic strain rate $\dot{\varepsilon}$ on a logarithmic scale. The flow curves show the trend of shifting toward the higher stress and lower strain rate region as the amount of strain increases. While the flow curve after the prestrain of 2% shows a large value of strain rate sensitivity at the low strain rate region, such a flow behavior disappears with the strain increment. As shown in Fig. 2, the region with a high strain rate shifts to a lower strain rate region when the amount of strain increases up to 50%. Finally, it is impossible to observe such a region when the prestrain increases over the strain of 100% at 515 °C. Shifting of flow curves toward a higher stress region with the increment of strain seemed to result from strain hardening due to deformation-enhanced grain growth.

The flow curve of the superplastic 7075 A1 alloy at high temperatures can be considered as a composite curve consisting of a GBS represented by a σ vs $\dot{g}$ curve and an accommodating GMD represented by a σ^{I} vs $\dot{a}$ curve. These two curves can then be separated from an overall flow curve because the GBS is not likely to occur at the lower stress end and also at the higher strain rate end. Once the GMD curve is determined, the

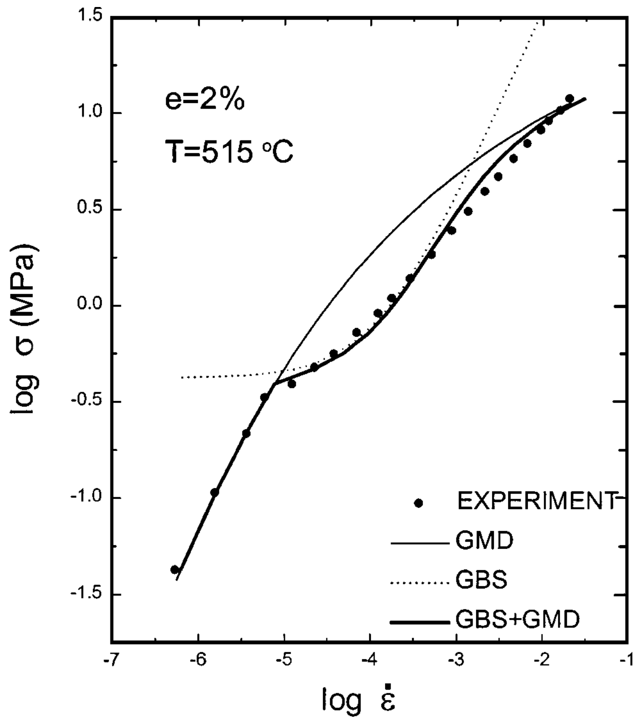

(a)

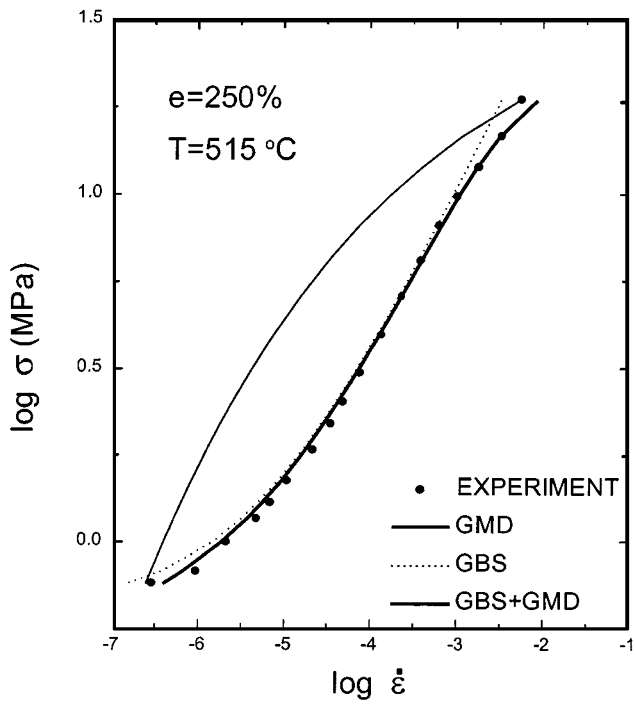

(b)

Fig. 3 The flow curve is separated into the GBS curve and GMD curve. (**a**) When the strain is 2%, a portion of GMD is shown. (**b**) As the strain amount increases, the GBS dominant region becomes to broad

GBS curve can then be determined by subtracting $\dot{a}$ from the total inelastic strain rate $\dot{\varepsilon}$ at each stress level, according to Eq 1. Also, the term represents the internal strain rate and disappears when the load relaxation test at high temperature is performed in a steady state.

The example of flow curve analysis is illustrated for the flow curves with $d = 7.1$ μm at 515 °C in Fig. 3(a). The solid line is first constructed by a nonlinear curve fitting method using only high and low stress end data, which are believed to proceed only with dislocation motion, to determine the three

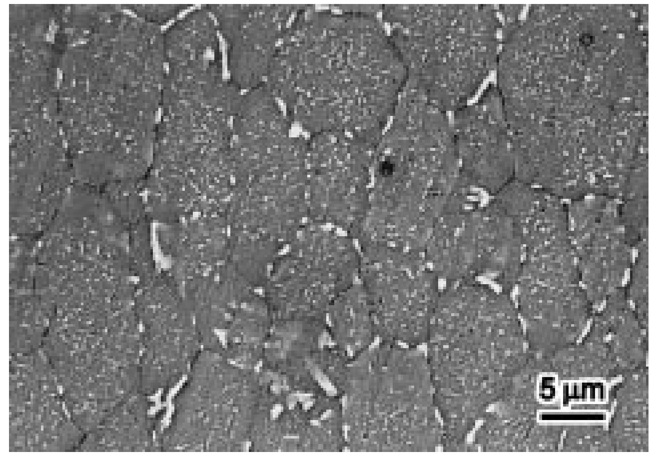

(a)

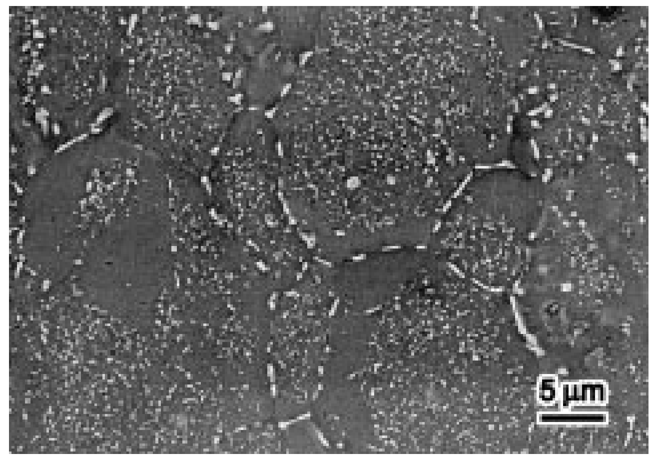

(b)

Fig. 4 The SEM micrographs of the deformed 7075 Al alloy. (**a**) Specimen deformed by 300% with $\dot{\varepsilon} = 1 \times 10^{-2}/s$ at 510 °C. (**b**) Specimen deformed by 600% with $\dot{\varepsilon} = 5 \times 10^{-4}/s$ at 510 °C

Table 1 The constitutive parameters determined from the load relaxation test results of a 7075 Al alloy with the increment of strain at 515 °C

	GMD			GBS		
%	Log σ^*	Log $\dot{\alpha}^*$	p	Log Σ_g	Log $\dot{g}_0$	M_g
2	1.70	−0.55	0.15	−0.38	−3.80	1.0
50	1.67	−1.95	0.15	−0.31	−4.85	0.61
150	1.67	−2.45	0.15	−0.26	−5.25	0.56
250	1.67	−2.51	0.15	−0.19	−5.30	0.51

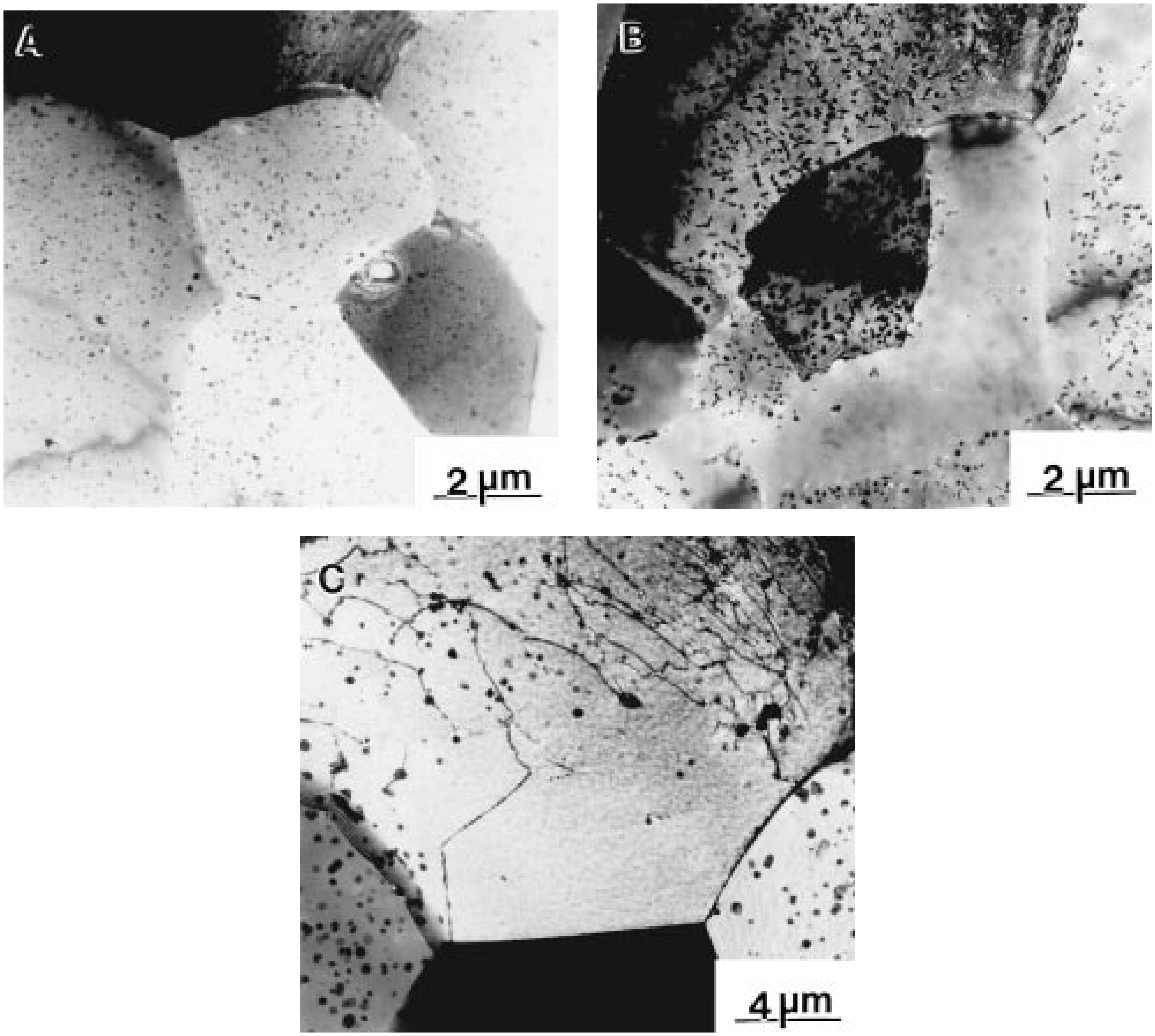

Fig. 5 TEM micrographs of the deformed 7075 Al alloy. (**a**) Recrystallized specimen. (**b**) Specimen deformed by 80% with $\dot{\varepsilon} = 1 \times 10^{-3}/s$ at 495 °C. (**c**) Specimen deformed by 80% with $\dot{\varepsilon} = 1 \times 10^{-2}/s$ at 495 °C

unknown constitutive parameters σ^*, $\dot{a}^*$, and p for the GMD curve in Eq 3. Then the GBS curve is extracted from the flow curve and used for a subsequent nonlinear curve fitting to determine another three unknown constitutive parameters Σ_g, $\dot{g}_0$, and M_g for the GBS curve. As the amount of strain increases, however, it becomes difficult to separate the GMD curve from the flow curve. After determining the GBS curve from the flow curve, we can obtain the GMD curve. In order to obtain more accurate and meaningful results, the nonlinear curve fitting was repeated several times until it became satisfactory (Fig. 3b). The constitutive parameters determined in this way are listed in Table 1. The heavy solid lines in Fig. 3 as well as those in Fig. 2 are the predicted composite curves produced by using the constitutive parameters listed in Table 1.

3.2 The Deformed Microstructure

Figure 4 shows the scanning electron microscopy (SEM) micrographs of the deformed specimen, which had tensile elongation of 300% under the strain rate of $\dot{\varepsilon} = 1 \times 10^{-2}/s$ (Fig. 4a) and 600% with the strain rate of $\dot{\varepsilon} = 5 \times 10^{-4}/s$ (Fig. 4b) at 510 °C, respectively. The tensile axis was in the vertical direction of all the photos. The grain shape became somewhat elongated in the direction of the tensile axis for the condition of higher strain rate, $\dot{\varepsilon} = 1 \times 10^{-2}/s$, compared with the equiaxed grains of the specimen deformed at the lower strain rate. Although both microstructures showed the particle free zones (PFZs), the width and direction of each PFZ differed. Some of particle free zones reach about 5 μm in Fig. 4(b).

The TEM micrographs of a 7075 Al alloy were also taken at several conditions, as shown in Fig. 5. Figure 5(a) shows the microstructure of the recrystallized grains with a homogeneous distribution of particles through the matrix. The round particles are the Cr-enriched dispersiods whose role is to restrict the grain migration during deformation at high temperatures. Figure 5(b) shows the microstructure of a gage section that was deformed by 80% with the strain rate of $\dot{\varepsilon} = 1 \times 10^{-3}/s$ at 495 °C. A number of precipitates are found to be segregated at some grain boundaries. It is also possible to observe wide PFZs adjacent to the grain boundaries. The formation of PFZs seems to be closely related with the grain boundary migration, which follows GBS.[6] When the specimen is deformed by 80% with the strain rate of $\dot{\varepsilon} = 1 \times 10^{-2}$ / s at 495 °C, it is possible to observe the dislocation activities, as shown in Fig. 5(c). The PFZs have been also observed in this condition.

4. Discussion

The constitutive parameters listed in Table 1 illustrate clearly the evolutions of the GBS and GMD characteristics with the increment of strain. The plastic hardness σ^* signifies the internal resistance to dislocation motions and has been known to have a modified Hall-Petch type relation with the grain sizes.[7] It is found from Table 1 that the plastic hardness σ^* for GMD remains almost constant with the strain. Hence, the grain size of the specimen seemed not to increase extensively within the strain range used in the present study. The grain size after 4 times load relaxation tests at 515 °C was found to be 8.3 μm. The critical stress for GBS, Σ_g, has also been known to increase with the grain size.[5,7] In this case, however, the increase of Σ_g is too drastic to attribute to the effect of grain size increment. Therefore, it appears to be related not only with the grain size directly but also with some other factors.

From the results of recent fundamental research on boundary sliding, it has been suggested that the boundary dislocations have to move in order for the boundary to slide.[8] If the grain boundary does not contain enough boundary dislocations, GBS is going to be impeded such as in the case of sliding on the small angle boundary. There have been several reports on the origin of grain boundary dislocation.[8,9,10] It has been observed that dissociation of lattice dislocations at high angle grain boundary occurs either by increasing the width of the dislocation core or by the formation of a large number of partial dislocations with small burgers vectors. Consequently, GBS occurs more easily along the destabilized grain boundaries that contain many grain boundary dislocations. The segregation of precipitates or solute atoms at the grain boundaries (Fig. 4 and 5) is likely to hinder the motion of grain boundary dislocations and consequently give a rise in the critical stress for GBS, Σ_g.

While the power exponent for the GMD constitutive equation has the constant value of $p = 0.15$ for all the conditions, the power index of GBS, M_g, becomes lower with the strain increment and finally obtains a value of about 0.5 after a certain amount of strain. The power index of GBS, M_g, determines the viscosity of the grain boundaries during GBS. According to the previous results performed in our laboratory, the single-phase superplastic aluminum alloys showed the value of 1 from the load relaxation test after a small amount of prestrain, while two-phase materials had the value of 0.5.[5,7,11] However, the evolution of the power index, M_g, with the increment of strain was first proved experimentally in the present study. It is thought

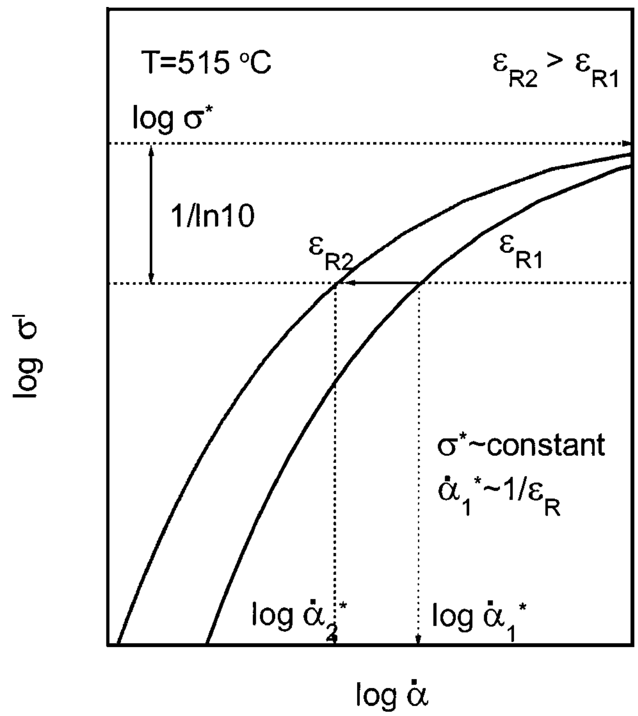

(a)

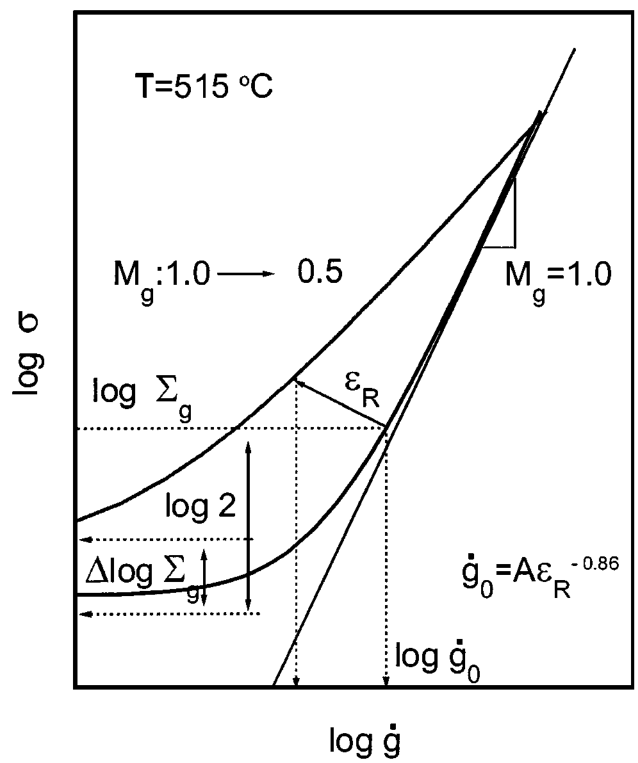

(b)

Fig. 6 The schematic representation of the effect of the strain increment: (**a**) GMD curve and (**b**) GBS curve

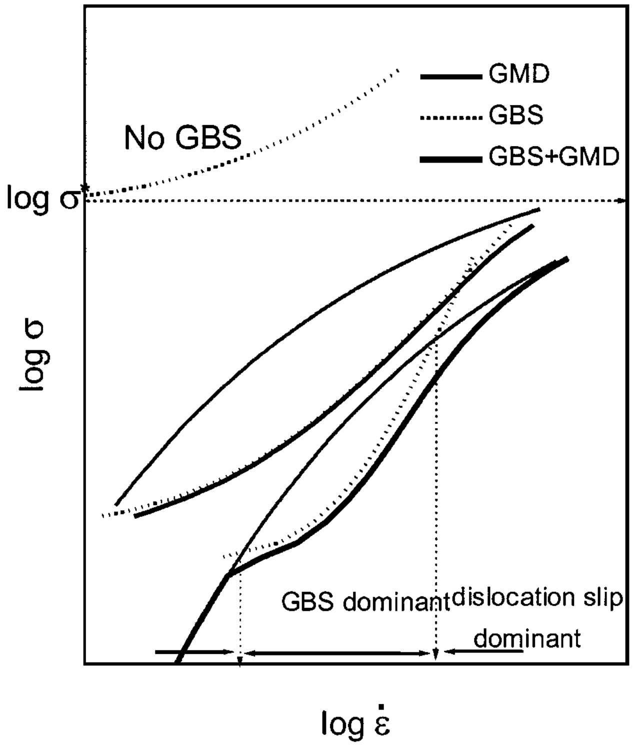

Fig. 7 The schematic representation of the effect of the strain increment on the superplastic deformation of a 7075 Al alloy

that the loss of a Newtonian viscous flow for GBS is closely related to the evolution of grain boundary structures. As stated previously, the viscosity of grain boundary seems to be related with the mobility of grain boundary dislocations. Consequently, the amount of solutes or particles and the diffusion coefficient of solute atoms might determine the variation of M_g with the increment of strain. When the value of M_g decreases to a specific value with the strain and remains constant after a certain strain, the grain boundaries seem to have a certain steady state for GBS process in the present 7075 Al alloy.

Because the plastic hardness σ* remains nearly constant, the GMD curve moves just horizontally toward the lower strain rate region due to the decrease of $\dot{a}^*$ with the increment of strain, as shown in Fig. 6(a). On the other hand, the shape of the GBS curve changes greatly due to the change of the power index M_g, as the deformation proceeds. Also, the critical stress Σ_g and the reference strain rate for GBS $\dot{g}_0$ vary with the increment of strain. Hence, the GBS curve moves to the higher stress and lower strain rate region with the strain (Fig. 6b).

When the GMD and GBS curves are brought together, the evolution of the entire deformation process with the increment of strain is as schematically illustrated in Fig. 7. It can be demonstrated that the strain rate region dominated by GBS becomes extended due to the increase of M_g with the increment of strain.

In summary, it is thought that the evolution of superplastic deformation characteristics with the increment of strain has a close relationship with the evolutions of grain boundary structures, such as grain boundary dislocations and segregation of precipitates at grain boundaries. However, an explicit explanation of the origin and characteristics of grain boundary dislocation has not been given in the present paper and still needs to be investigated.

5. Conclusions

- The flow curves of a 7075 Al alloy could be effectively analyzed by separating them into the GMD and GBS curves irrespective of the amount of strain.
- Compared with the GMD characteristics with the strain accumulation, there have been many changes in the characteristics of GBS with the increment of strain. The Newtonian viscous flow, which is characterized by a power index of $M_g = 1$, is predicted in the early stage of deformation. As the strain is accumulated, the value index becomes smaller, $M_g = 0.5$, after a certain amount of strain.
- The motion of grain boundary dislocations seems to be inhibited by the segregation of solute atoms and particles at the grain boundaries. Consequently, the viscosity of grain boundaries becomes lower with the increment of strain, before the grain boundaries reach a certain steady state.

References

1. A.H. Chokshi, A.K. Mukherjee, and T.G. Langdon: *Mater. Sci. Eng.*, 1993, vol. R10, pp. 237-74.
2. D.S. Wilkinson and C.H. Caceres: *Acta Metall.*, 1984, vol. 32, pp. 1335-45.
3. C.C. Bampton and J.W. Edington: *Metall. Trans. A*, 1982, vol. 13A, pp. 1721-27.
4. M.K. Rao and A.K. Mukherjee: *Mater. Sci. Eng.*, 1986, vol. 80, pp. 181-93.
5. T.K. Ha and Y.W. Chang: *Acta Mater.*, 1998, vol. 46 (8), pp. 2741-49.
6. A.D. Sheikh-Ali and R.Z. Valiev: *Phys. Status Solidi (a)*, 1990, vol. 117, pp. 429-36.
7. T.K. Ha and Y.W. Chang: *Scripta Metall. Mater.*, 1995, vol. 32, pp. 809-13.
8. M.F. Ashby: *Surf. Sci.*, 1972, vol. 31, pp. 498-542.
9. R.Z. Valiev, V.Y. Gertsman, and O.A. Kaibyshev: *Phys. Status Solidi (a)*, 1986, vol. 97 (11), pp. 11-56.
10. T. Watanabe: *Mater. Sci. Forum*, 1997, vol. 233–234, pp. 375-82.
11. T.K. Ha and Y.W. Chang: *Scripta Metall. Mater.*, 1996, vol. 35, pp. 1317-23.